Research Article | Vol. 25, No. 17 | 21 Aug 2017 | OPTICS EXPRESS 20274
Optics EXPRESS

Beam shaping with tip-tilt varifocal mirror for indoor optical wireless communication

COREY POLLOCK,[1] JESSICA MORRISON,[2] MATTHIAS IMBODEN,[3] THOMAS D.C. LITTLE,[2] AND D.J. BISHOP[1,2,4,5]

[1]Department of Mechanical Engineering, Boston University, Boston, Massachusets, USA
[2]Department of Electrical and Computer Engineering, Boston University, Boston, Massachusets, USA
[3]'Ecole Polytechnique Fédérale de Lausanne (EPFL), Neuchâtel, Switzerland
[4]Division of Material Science and Engineering, Boston University, Boston, Massachusets, USA
[5]Department of Physics, Boston University, Boston, Massachusets, USA
*cpollock@bu.edu

Abstract: MEMS mirrors are currently used in many applications to steer beams of light. An area of continued research is developing mirrors with varifocal capability that allows the beam to be shaped and focused. In this work, we study the varifocal capability of a 380 μm diameter, thermally actuated MEMS mirror with a ± 40° tip-tilt angle and a radius of curvature between -0.48 mm to 20.5 mm. Light is coupled to the mirror via a single mode optical fiber, similar to an indoor optical wireless communication architecture. The performance of the mirror is characterized with respect to (1) the profile of the reflected beam as the mirror deforms and (2) the mirror's impact when integrated into an optical communication system. We found that the mirror can focus light to a beam with a 0.18° half-angle divergence. Additionally, the ability to change the shape of fiberized light from a wide to narrow beam provides an unmatched level of dynamic control and significantly improves the bit error rate in an optical communication system.

OCIS codes: (230.3990) Micro-optical devices; (230.4040) Mirrors; (220.1080) Active or adaptive optics; (060.2605) Free-space optical communication; (060.2390) Fiber optics, infrared.

References and links

1. V. Milanović, A. Kasturi, and V. Hachtel, "High Brightness MEMS Mirror Based Head-Up Display (HUD) Modules with Wireless Data Streaming Capability," Proc. SPIE **9375**, 93750A (2015).
2. J. Reitterer, F. Fidler, G. Schmid, T. Riel, C. Hambeck, F. Saint Julien-Wallsee, W. Leeb, and U. Schmid, "Design and evaluation of a large-scale autostereoscopic multi-view laser display for outdoor applications," Opt. Express **22**, 27063–27068 (2014).
3. P. F. Van Kessel, L. J. Hornbeck, R. E. Meier, and M. R. Douglass, "A MEMS-based projection display," in *Proceedings of IEEE* (IEEE, 1998), vol. 86, pp. 1687–1704.
4. M. Strathman, Y. Liu, X. Li, and L. Y. Lin, "Dynamic focus-tracking MEMS scanning micromirror with low actuation voltages for endoscopic imaging," Opt. Express **21**, 23934–23941 (2013).
5. L. Li, R. Li, W. Lubeigt, and D. Uttamchandani, "Design, simulation, and characterization of a bimorph varifocal micromirror and its application in an optical imaging system," J. Microelectromech. Syst. **22**, 285–294 (2013).
6. C. D. Lu, M. F. Kraus, B. Potsaid, J. J. Liu, W. Choi, V. Jayaraman, A. E. Cable, J. Hornegger, J. S. Duker, and J. G. Fujimoto, "Handheld ultrahigh speed swept source optical coherence tomography instrument using a MEMS scanning mirror," Biomed. Opt. Express **5**, 293–311 (2013).
7. P. Brandl, S. Schidl, A. Polzer, W. Gaberl, and H. Zimmermann, "Optical Wireless Communication With Adaptive Focus and MEMS-Based Beam Steering," IEEE Photon. Technol. Lett. **25**, 1428–1431 (2013).
8. A. Gomez, K. Shi, C. Quintana, G. Faulkner, B. C. Thomsen, and D. O'Brien, "A 50 Gb/s Transparent Indoor Optical Wireless Communications Link With an Integrated Localization and Tracking System," J. Lightwave Technol. **34**, 2510–2517 (2016).
9. J. Morrison, M. Rahaim, Y. Miao, M. Imboden, T. D. C. Little, V. Koomson, and D. J. Bishop, "Directional Visible Light Communication Signal Enhancement Using a Varifocal Micromirror with Four Degrees of Freedom," Proc. SPIE **9954**, 99540C (2016).
10. C. W. Oh, Z. Cao, E. Tangdiongga, and T. Koonen, "Free-space transmission with passive 2D beam steering for multi-gigabit-per-second per-beam indoor optical wireless networks," Opt. Express **24**, 19211–19227 (2016).
11. T. Sasaki and K. Hane, "Varifocal micromirror integrated with comb-drive scanner on silicon-on-insulator wafer," J. Microelectromech. Syst. **21**, 971–980 (2012).

#298083 https://doi.org/10.1364/OE.25.020274
Journal © 2017 Received 14 Jun 2017; revised 19 Jul 2017; accepted 3 Aug 2017; published 11 Aug 2017

Optics EXPRESS

12. R. Hokari and K. Hane, "Micro-mirror laser scanner combined with a varifocal mirror," Microsys. Technol. **18**, 475–480 (2012).
13. J. Morrison, M. Imboden, T. D. C. Little, and D. J. Bishop, "Electrothermally actuated tip-tilt-piston micromirror with integrated varifocal capability," Opt. Express **23**, 9555–9566 (2015).
14. V. Jungnickel, A. Fork, T. Haustein, U. Kruger, V. Pohl, and C. von Helmolt, "Electronic Tracking For Wireless Infrared Communications," IEEE Trans. Wireless Commun. **2**, 989–999 (2003).
15. J. C. Chau, C. Morales, and T. D. C. Little, "Using Spatial Light Modulators in MIMO Visible Light Communication Receivers to Dynamically Control the Optical Channel Using Spatial Light Modulators in MIMO Visible Light Communication Receivers to Dynamically Control the Optical Channel," in *Proceedings of the 2016 International Conference on Embedded Wireless Systems and Networks* (Junction Publishing, 2016), pp. 347–352.
16. K. Wang, A. Nirmalathas, C. Lim, and E. Skafidas, "High-Speed Optical Wireless Communication System for Indoor Applications," IEEE Photon. Technol. Lett. **23**, 519–521 (2011).
17. H. Zappe, *Fundamentals of Micro-Optics* (Cambridge University Press, 2010), 1st ed.
18. R. Paschotta, "Focal Length," https://www.rp-photonics.com/focal_length.html.
19. M. T.-K. Hou and R. Chen, "Effect of width on the stress-induced bending of micromachined bilayer cantilevers," J. of Micromech. Microeng. **13**, 141–148 (2002).
20. L. Couch, *Digital and Analog Communication Systems* (Pearson, 2007), 7th ed.

1. Introduction

Microelectromechanical systems (MEMS) are used in a wide range of optical applications, such as displays [1–3], biomedical imaging [4–6], and communications [7–10]. Most current research and commercially available MEMS mirrors utilize a flat design and typically employ passive optics to shape the beam. The mirror then directs the beam to a detector or camera. One limitation of the existing systems is that they are confined to a fixed focal length and/or beam size. An area of current research is developing mirrors which have the capability to change their focal length, and consequently their beam size [11, 12]. We have developed a thermally actuated varifocal mirror, shown in Fig. 1, that has a ± 40° tip-tilt range and also has a tunable radius of curvature (ROC) range of -0.48 mm to 20.5 mm [13]. This allows a beam to be steered around a room at ± 40° optical while at the same time, the beam diameter can be less than 5 mm or greater than 50 mm at a distance of 0.5 m from the mirror. This paper focuses primarily on the varifocal feature of the mirror and demonstrates that using the varifocal degree of freedom can improve indoor optical wireless communication (OWC).

Using a narrow beam will improve the signal to noise ratio (SNR) and lead to faster data transmissions. Because of the SNR considerations, OWC requires the ability to beam steer. The device shown here is a practical, low cost way of doing this. There are, however, some situations when having a larger beam could be beneficial, such as when the transmitter is first locating the receiver, or when it is tracking a receiver as it moves [14, 15]. Varifocal capability provides dynamic control of the beam size to continuously optimize the beam for the specific scenario. One of the common architectures for OWC is with a fiber delivery (fiberized) system [10, 16]. This consists of a centralized communications system that can then deliver light to the transmitters via optical fibers compared to having each transmitter integrated with its own light source. This mirror's large tunable focal range allows it to be integrated into a fiberized system without additional optics, leading to more compact designs.

2. Setup/method

The mirror, shown in Fig. 1, is fabricated using the MEMSCAPs multi-user PolyMUMPS process. It consists of three layers of polysilicon followed by a layer of gold. The mirror consists of eight wedge shape, polysilicon-gold sections. A residual tensile stress in the gold due to the evaporation process provides an initial curvature to the mirror. Applying a current through the polysilicon springs heats the springs and via thermal conduction heats the eight mirror sections. This heats the eight mirror sections uniformly and causes their curvature to decrease, flattening the mirror in unison due to the different thermal expansion coefficients of gold and polysilicon.

Optics EXPRESS

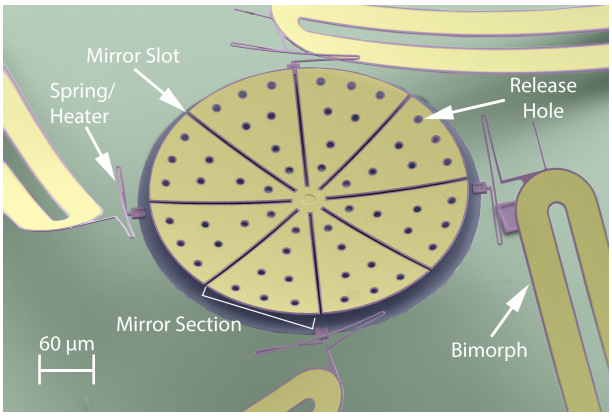

Fig. 1. False color SEM image of thermally actuated varifocal mirror connected to four thermal bimorphs via serpentine springs.

This changes the ROC and therefore the focal point of the mirror [13].

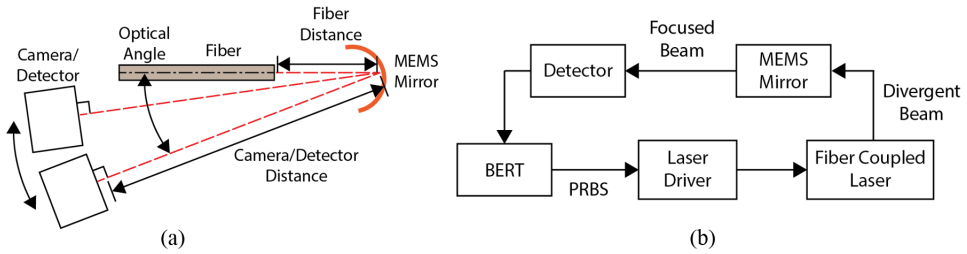

Fig. 2. (a) Illustration (not to scale) of test setup demonstrating that the detector is always normal to the reflected beam and is always the same distance from the mirror. (b) System schematic of the bit error rate tester (BERT) system used for collecting bit error rate (BER) data. A PXIe-6555 generates a PRBS which is used to control the laser driver and subsequently the fiber coupled laser. The light is focused using the MEMS mirror onto the detector whose signal is compared to the original PRBS signal in the PXIe-6555.

This experimental setup emulates a fiberized system as shown in Fig. 2. It uses 1550 nm light coupled into a single mode optical fiber with a core diameter of 8.2 μm and outputs a Gaussian beam with a measured half angle divergence of 4.6°. The fiber is positioned with a relatively small initial angle to the mirror (1°-3°). To maximize the power from the mirror for subsequent experiments, the optimal distance between the fiber and the mirror is measured. This optimal fiber position is dependent on the incident beam divergence angle and the specific mirror geometry (i.e. mirror radius, slots and holes as shown in Fig. 1). This experiment used a germanium photodiode power detector with a 9.5 mm diameter sensor placed 90 mm from the mirror. Light from the fiber was focused by the mirror and directed toward the detector without any additional lens or filters. The measured data is compared to a Zemax simulation based on ray optics and a mathematical model of the mirror as shown in Fig. 3. The mathematical model approximates the mirror as a circle with wedge shaped slots which takes into account both the area of the slot and release holes of each mirror section. The power of a Gaussian beam is integrated over the approximated

Optics EXPRESS

surface to provide the reflected optical power. In this plot, the efficiency is defined as: $\eta = \frac{P_r}{P_t}$, where η is is efficiency, P_r is the power received at the detector and P_t is the power transmitted from the fiber. Although the measured optimal distance between the fiber and the mirror agrees with the theory and simulations, the measured peak efficiency is only 83% of the theory and simulations. As the fiber gets within 0.75 mm of the mirror, the efficiency does not improve as do the simulations. These discrepancies may result from two limitations/differences in the simulated models versus the experimental setup. First, simulations show that a misalignment of 30 μm between the fiber and the mirror has a larger effect on efficiency at distances closer than 0.75 mm. This could explain why the simulated efficiency increases, whereas the measured efficiency decreases at fiber distances closer than 0.75 mm. This result is shown in Fig. 3. Second, both the Zemax and mathematical models, place the detector close enough to capture all the reflected light. Due to physical limitations of the test equipment, the detector is placed at a further distance and the beam is focused using the mirror. Another possible explanation for this efficiency loss is by diffraction from the mirror. The Airy disk from a circular diffraction pattern contains 84% of the total optical power, which would account for the discrepancy between the simulation and data [17]. Although the measured efficiency is significantly lower than the simulated result, an important finding from the simulation is that the absolute maximum efficiency of this mirror geometry is 80%. This could in principle be improved by removing the mirror's release holes and reducing the size of the slots. By removing these features, the efficiency approaches the reflectivity of the mirror material until the fiber is far enough away that the beam size is larger than the mirror. This theoretical limit without release holes and slots is plotted in Fig. 3. This is important for future designs and studies. Based on these results, all future experiments are performed with a fiber-mirror separation of 1.275 mm.

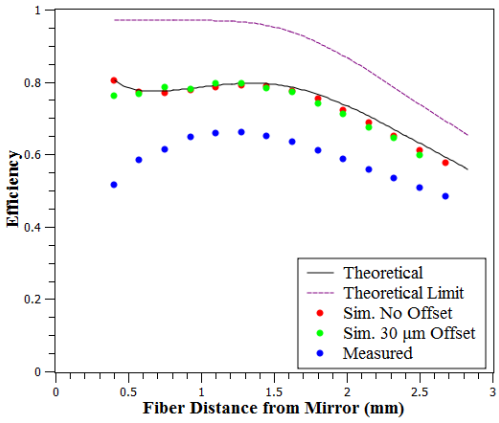

Fig. 3. Plot of the optical efficiency versus the distance between the end of the fiber and the mirror. Efficiency is defined as the ratio between the power reflected from the mirror and the power measured from the fiber. Included is a theoretical math model, limit of the theoretical math model as the holes and slots are removed, simulation results with no misalignment between the fiber and mirror, a 30 μm misalignment, and measured data.

All testing of the mirror discussed here falls under two categories: characterizing the beam profile and characterizing the bit error rate (BER) with respect to a) the power applied to the mirror (i.e. radius of mirror curvature), b) the optical angle of the beam, and c) the distance from the mirror to the detector. Unless otherwise stated, all testing used the setup illustrated in Fig. 2. While characterizing the mirrors performance compared to angle, this setup maintained a fixed distance between the mirror and the detector. The setup also ensures that the light from the

Optics EXPRESS

mirror arrives at an angle normal to the detector as shown in Fig. 2. This allows the beam to be characterized with respect to the angle and shape of the reflected beam independently from the detector's position and orientation. A DataRay WinCamD-UHR camera with phosphor coating and a 5.2 mm x 5.2 mm sensor was used to collect the beam profile data. BER data was measured using an InGaAS variable-gain avalanche photodetector with a 400 MHz bandwidth and a 0.2 mm diameter sensor as part of the system illustrated in Fig. 2. The system consists of a bit error rate tester (BERT) to generate and analyze a 20 bit pseudorandom binary sequence (PRBS) at 100 Mbps, a laser driver board, and the aforementioned detector. The peak optical output of the optical fiber was approximately 1 mW. In most cases during communication testing, this led to an error free connection (BER $< 10^{-9}$). To better characterize the performance of the mirror, a series of neutral density (ND) filters are used to attenuate the signal to achieve BER values of 10^{-9} or greater. Table 1 summarizes the important equipment specifications and system parameters for the BER testing. In addition to measuring beam profiles directly, the setup was simulated using a combination of an optical surface profiler and Zemax OpticStudio to obtain a better understanding of the mirror's shape and its effect on the beam profile. The mirror was first analyzed at different power levels using the profiler and then modeled in Zemax.

Table 1. Typical BER Testing Parameters

Detector	
BandWidth	DC - 400 MHz
Sensor Type	InGaAs Avalanche Photodetector
Sensor Size	⌀ 0.2 mm
BERT	
Modulation	100 Mbps
Word	20 bit PRBS
Peak Optical Power	1.1 mW
Setup	
Fiber-Mirror Distance	1.275 mm
Mirror-Detector Distance	90 - 1,000 mm
Fiber-Detector Angle	7° - 20°
ND Filters	0.5%, 1.0%, 3.0%, and 5.0% transmission
Mirror Power	10 - 12 mW

3. Results

3.1. Measured beam profile

Using the DataRay camera, the beam profile is characterized with respect to mirror power, angle, and distance. For all measurements, the diameter is defined to be where the beam intensity falls to 13.5% of the peak value, also known as the $1/e^2$ width. As the mirror radius changes, the beam transitions from defocused, to focused, and back to defocused as shown in Fig. 4. Prior to testing, the profiler was used to establish the relationship between the mirror power and the mirror's ROC. The minimum beam diameter is achieved at a power of approximately 12.9 mW which corresponds to an ROC of approximately 2.5 mm. A spherical mirror's theoretical focal length is $f=(R/2)$, where f is the focal length and R is the radius of curvature. Therefore, if the fiber is approximated as a point source and given that the fiber is positioned 1.275 mm from the mirror, it is expected that the beam would be collimated at an ROC of 2.55 mm. This puts the measured optimal ROC within 2% of the theoretical. As the optical angle increases, the power needed for the minimum diameter along the x and y axes began to drift apart to approximately 13.1 mW and 12.6 mW as shown in Fig. 4, which corresponds to 2.54 mm and 2.46 mm respectively. This

Optics EXPRESS

separation of the ROC for each axis is a product of a spherical mirror geometry. The earlier relationship between radius of curvature and focal length applies only to a spherical mirror normal to the incident beam. If there's an angle between the beam and the mirror, the focal length becomes $f_{tan} = (\frac{R}{2})\cos(\theta)$ in the tangential direction and $f_{sag} = \frac{R}{2\cos(\theta)}$ in the sagittal direction [18]. Applying these equations to the original measured data, the theoretical radius of curvature should be 2.54 mm and 2.46 mm for the x and y axis respectively, which matches the measured values.

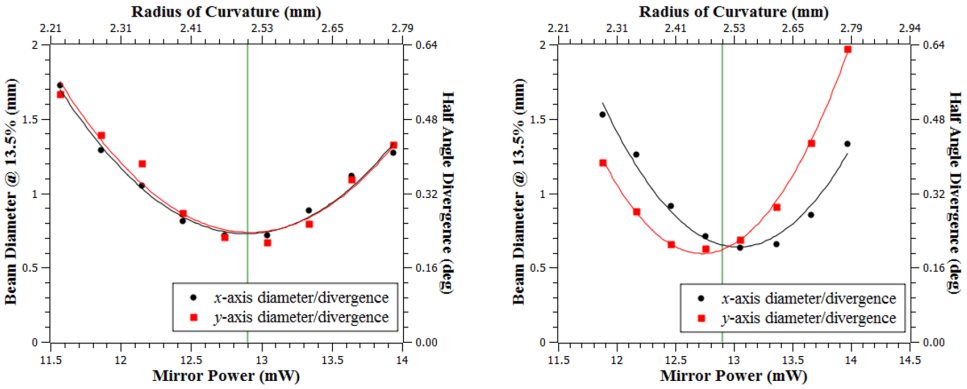

Fig. 4. Beam size versus the power to heat the mirror which corresponds to the mirrors radius of curvature. The vertical green line in both plots represent the position of the minima in (a) for comparison. The camera is 90 mm from them mirror. (a) Characterization with an optical angle of 5 degrees. (b) Characterization of the beam with an optical angle of 20 degrees.

One of the advantages of this MEMS mirror is its ability to access large tilt angles. For the results in Fig. 4, the optical angle was changed by manually moving the optical fiber with respect to the mirror. On the other hand, the data shown in Fig. 5 was measured by titling the mirror with a bimorph. This requires that the bimorph be heated and this extra heat affects the mirror's ROC, resulting in a larger beam size. The inconsistent beam size is a problem for many applications that demand precise control over the beam size. However, as Fig. 5 shows, this problem can be overcome by optimizing the mirror power for a given beam size as the bimorph actuates. In this experiment the mirror power was optimized for the smallest beam size. This effectively compensates for the added heat and the mirror maintains the optimal curvature. When controlled correctly, the angle between the incident beam and the mirror has little effect on the reflected beams performance.

One of the potential applications for this mirror is OWC, in which case the relevant distance range for the detector is up to 3 m [10, 16]. As the distance to the camera increases, the minimum beam size also increases in a linear fashion with a minimum half-angle divergence of approximately 0.18°. We believe that the reason the angle isn't smaller is because the system is approaching the diffraction limit of the mirror. At 3 m the expected beam diameter is approximately 18 mm. Figure 6 includes a comparison of the achievable beam diameters at each distance for the MEMS mirror, the optical fiber and a collimated beam as used by [10]. It also illustrates the mirror's capability to vary the beam size at a given distance, but it also demonstrates the ability to maintain a beam size at different distances. Since the collimated beam and optical fiber

Optics EXPRESS

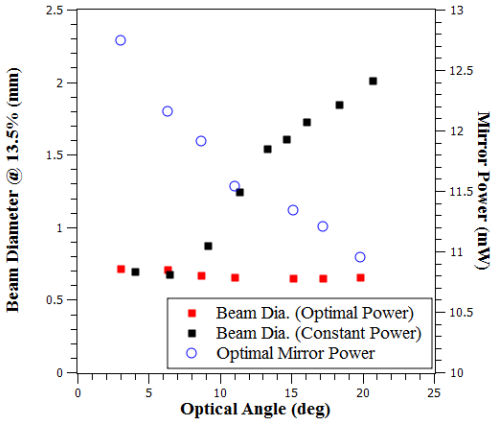

Fig. 5. The beam diameter versus optical angle. If the mirror power is held constant while the bimorph is actuating, the mirror's radius of curvature changes and the beam size increases. Optimizing the power at each tilt angle allows the beam size to stay relatively constant. The camera is 90 mm from the mirror.

are static systems they each only have a single diameter at each distance, whereas the MEMS mirror has a range. The plot includes a measured range and a theoretical range for the mirror. The measured range includes diameters that were directly measured between 100 mm and 1 m from the mirror and then extrapolated to 3 m. At these distances (i.e. 100 mm, 250 mm, 500 mm and 1,000 mm), the mirror was actuated, which focuses and de-focuses the beam, to measure the smallest beam diameter, as well as a range of other sizes. Past 1 m, the beam diameter is larger than the detector and could not be measured. As shown in [13], the mirror can completely flatten and can even invert its radius of curvature. Based on these measurements we show that the beam size has a theoretical range that continues past the measured data and then up to and slightly beyond the size of the optical fiber.

3.2. Simulated beam profile

To obtain a better understanding of the system, the setup was simulated using Zemax OpticStudio. The mirror was modeled using a modified Zernike surface defined by:

$$z = \frac{cr^2}{1+\sqrt{1-(1+k)c^2r^2}} + \sum_{i=1}^{8} \alpha_i r^{2i} + \sum_{i=1}^{N} A_i Z_i(\rho, \phi)$$

where z is the surface height, c is the curvature of the surface, k is the conic constant, the α_i terms are aspheric coefficients, N is the number of Zernike coefficients in the series, A_i is the coefficient for the i^{th} Zernike polynomial, r is the radial coordinate in lens units, ρ is the normalized radial coordinate, and ϕ is the angular coordinate. During the analysis, there was a repeated error between the scanned and the modeled mirror surface due to curvature across the width of each mirror section. In a bimorph with a small width/length ratio, the effect of curvature in the width is small in comparison to the length. However, in larger width/length ratio structures, such as the mirror sections, there will also be curvature at the edges and tips, as shown in [19]. To correct for this error, a $B_1 \sin(8\phi + B_2)$ term was added to the above equation, where B_1 is a coefficient term and B_2 is angle offset. This compensates for some of the error between the mirror and model, and therefore improves the agreement between the simulated and measured profiles. The resulting measured and simulated profiles are shown in Fig. 7 as a comparison.

Optics EXPRESS

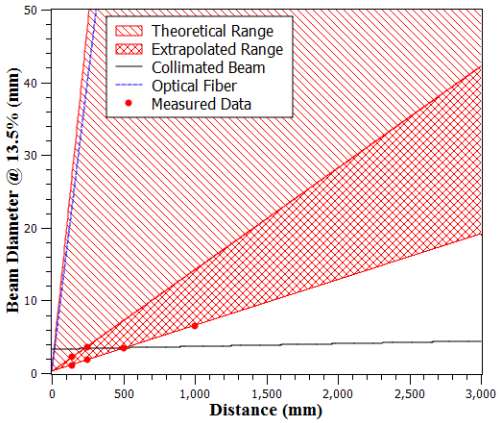

Fig. 6. Comparison between the MEMS mirror, a collimated beam (0.017° half angle [10]) and an optical fiber (4.6° half angle) with respect to beam diameter versus distance. The optical fiber and collimated beam have a single beam size at each distance whereas the varifocal mirror can achieve a range of sizes. The extrapolated range is based on the measured data points. The theoretical range encompasses the extrapolated range, as well as beam sizes that couldn't be measured directly but in principle the mirror could achieve based on the mirror's shape, demonstrated in [13].

Figure 8 plots the results of a series of these profiles to demonstrate that the simulated beam diameters follow a similar trend to the measured data. Although there is a large spread among the data, the trend shows that the minimum diameter is roughly equivalent to the measured data. This simulation shows that although the mirror may be approximated as spherical [13], there are deviations from this model which may have an effect on the mirrors efficiency.

Optics EXPRESS

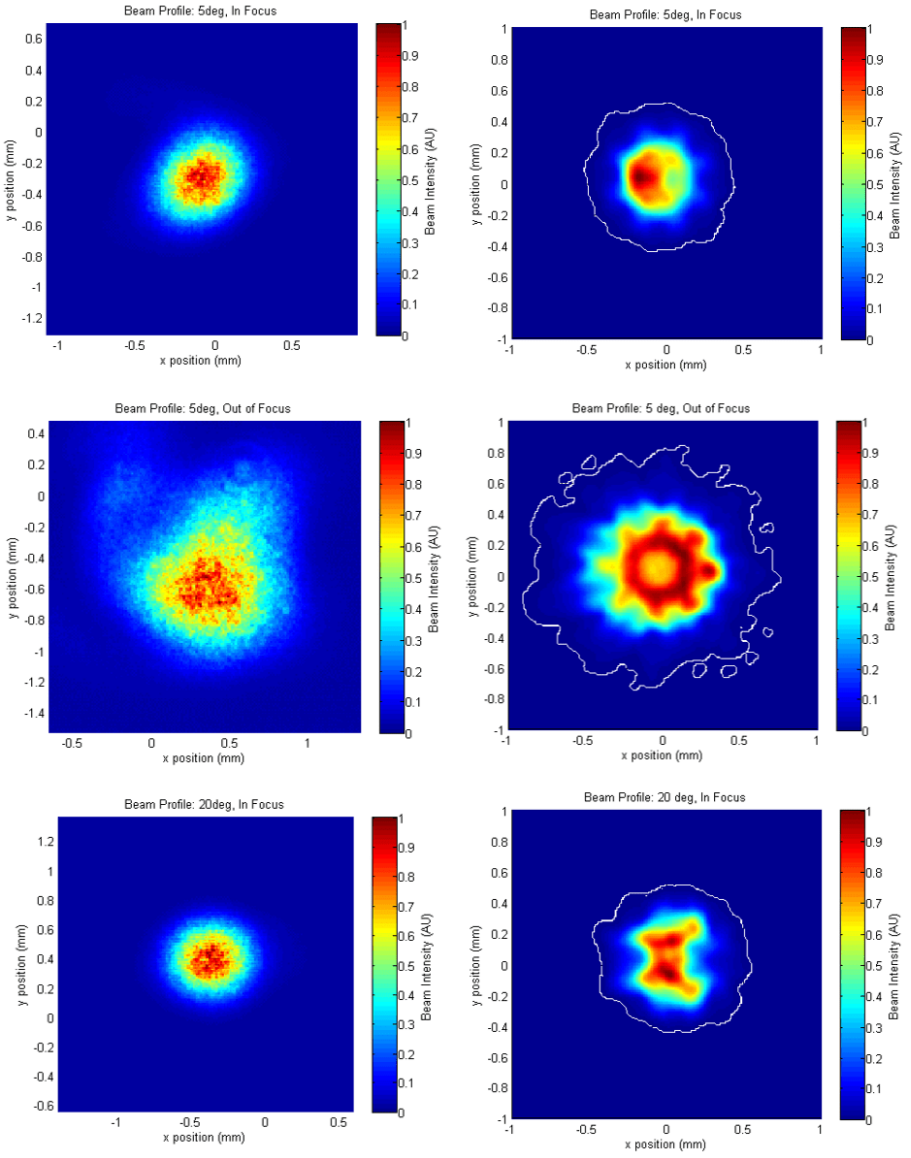

Fig. 7. Comparison of the measured and simulated beam profiles. The profiles on the left are measured profiles under three conditions: focused at a low angle, defocused at a low angle, and focused at a larger angle. The profiles on the right are the simulated counterparts to the measured profiles.

Optics EXPRESS

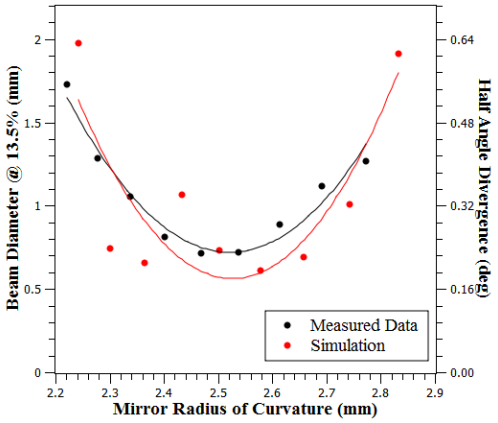

Fig. 8. Comparison of the x-axis beam diameter measured data and Zemax simulation. The measured data is repeated from Fig. 4 (a). The camera is 90 mm from the mirror.

3.3. Bit error rate testing

In the application of optical communications, the BER is directly related to the SNR. For an on-off keying system with Gaussian noise, the relationship is $BER = Q(SNR)$, where Q is the complimentary error function and $SNR = (\frac{S_d}{2\sigma})$, where S_d is the difference between the 1 and 0 signal and σ^2 is the variance of the noise [20]. Focusing the beam to a smaller spot size concentrates more of the optical power onto the detector and will increase the SNR, thus improving the BER of the system. Likewise, a larger beam diameter results in less optical power reaching the detector, decreasing the SNR and increasing the BER. To demonstrate this principle and verify that the mirror improves the BER, the BER is characterized with respect to the mirrors ROC and the resulting beam size. Figure 9 compares the BER to the beam diameter and demonstrates that they both are minimized at the same mirror curvature. As the mirror curvature changes, the BER improves until it reaches the smallest spot size at which point the BER increases again, validating the model and the predicated relationship between the signal intensity and BER.

Optics EXPRESS

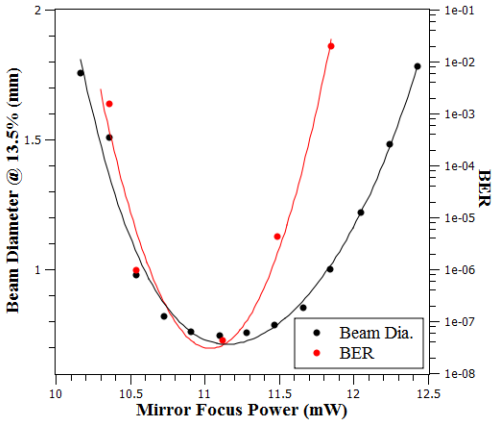

Fig. 9. Comparison of the beam diameter and the BER relative to the mirror power. This shows that as the beam diameter decreases the BER also decreases. Using the mirror to focus the beam to a smaller spot size significantly improves the BER. The BER experiment used a ND filter that allowed 0.5% of the light to be transmitted. Both the camera and detector are 90 mm from the mirror.

In a communication system where the detector's location can move, such as a phone or a laptop, it is important to have a device that can steer a beam. The scenario of a misaligned detector is illustrated in Fig. 10. In contrast to the rest of the experiments, here the detector is kept stationary as the mirror is actuated to steer the beam across the detector as shown in Fig. 10. When the beam is on center, the BER is at its minimum. Similar to [16], we find that as the beam moves off center in either direction, the BER increases. The ability to focus the beam on the center of the detector has a significant impact on the signal strength and the BER. When aligned and focused we obtain error free transmission.

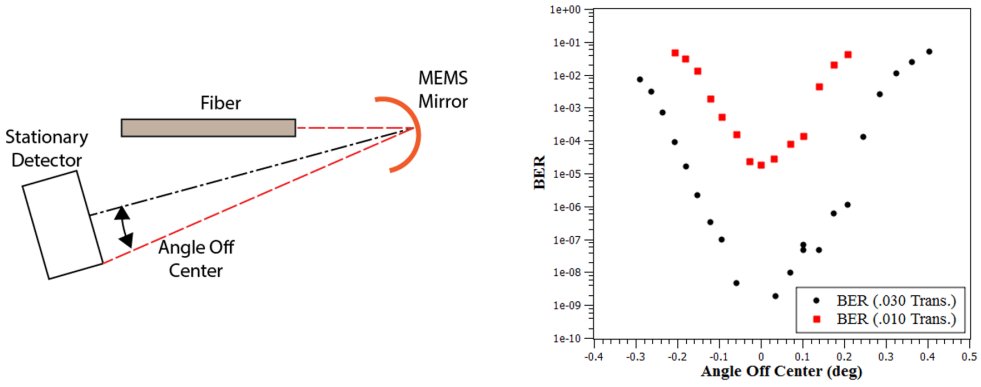

(a) (b)

Fig. 10. (a) Illustration (not to scale) of setup used to test the effect of sweeping a beam across a stationary detector.(b) BER as the beam moves away from the center of the detector. This plot includes data using two different filter setups. The black circles are data using a filter that allowed 3% of the light to be transmitted and the red squares used a filter that allowed 1% of the light to be transmitted. The detector is 250 mm from the mirror.

Optics EXPRESS

4. Conclusion

This paper characterizes the beam shaping and communication performance of a large focal range MEMS mirror. This focal range combined with the large tip-tilt angle provides this device with a unique level of dynamic control with regard to both beam steering and shaping allowing it to tune the light dynamically. This micromirror may be approximated as spherical and is capable of focusing light to a beam with a 0.18° half-angle divergence. Thus, at a distance of 3 m the mirror can focus the fiberized beam to an 18 mm diameter spot, which is approaching the diffraction limit of this mirror design. The ability to change the shape of fiberized light from a wide to a narrow beam provides a level of dynamic control in an optical communication system that cannot be achieved using current flat mirror systems.

Funding

National Science Foundation (NSF) (0812056)

Acknowledgments

This work was supported primarily by the Engineering Research Centers Program of the National Science Foundation under NSF Cooperative Agreement No. EEC-0812056. Any opinions, findings and conclusions or recommendations expressed in this material are those of the author(s) and do not necessarily reflect those of the National Science Foundation.